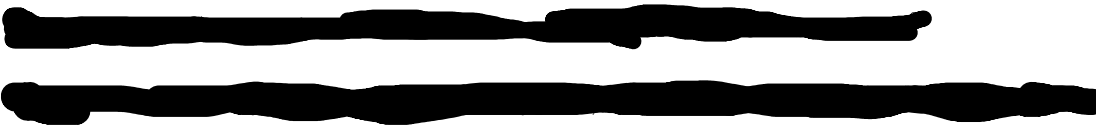


Brownian Motion



Abstract:

Brownian motion refers to the erratic movement observed in small particles suspended in a fluid or gas. These particles exhibit random and uncorrelated motion, prompting the question of the origin of their movement. Answering this question holds significant physical importance, as it provided the initial evidence for the existence of atoms and facilitated the experimental measurement of key physical constants such as the Boltzmann constant and Avogadro number. In this laboratory exercise, our objective is to observe Brownian motion in polystyrene microspheres in water and utilize our findings to calculate Boltzmann's constant. We will conduct this calculation using two samples containing microspheres of different diameters, utilizing the principles of the kinetic theory of gases.

Key-words: Brownian Motion, Random Walk, Statistical Mechanics, Microscopy, Particle tracing, Boltzmann constant, YOLOv8.

Introduction and Theoretical Overview

Brownian motion represents the irregular movement observed in small particles suspended in a fluid or gas. Contemporary understanding, substantiated by experimental confirmation, attributes Brownian motion to collisions between molecules of the surrounding substance and the suspended particles. When these particles are sufficiently small, making collisions non-negligible, their motion appears random. The inherent randomness stems from the countless collisions occurring each second, rendering deterministic calculations impractical. The random walk model serves as an effective statistical description of Brownian motion. Examples of Brownian motion are illustrated in Figures 1 and 2.

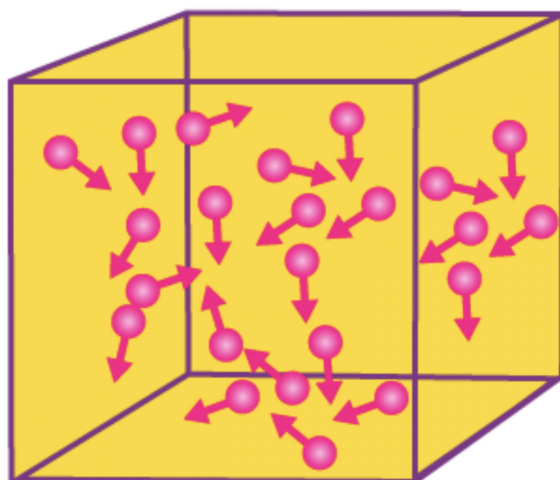


Figure 1: Brownian motion from atomic collisions

3D Plot: X-Y Coordinates=f(t) (XY-plane)

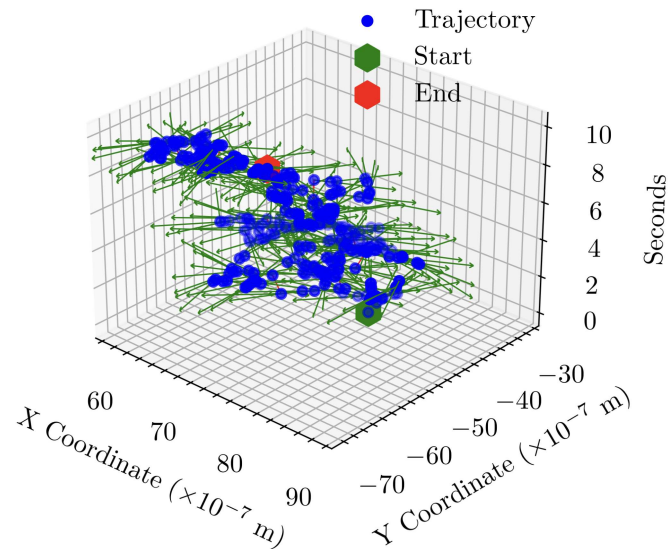


Figure 2: Brownian motion from atomic collisions of a single 1 μ m particle.

To analyze Brownian motion, we employ arguments from statistical mechanics and the kinetic theory of gases. These arguments aim to predict the behaviour of certain measurable quantities' mean values, such as the mean distance from the origin, the mean square distance from the origin, and the mean particle speed. These predictions establish connections between the mean values and specific physical quantities and constants. Consequently, by observing the motion of numerous particles undergoing Brownian motion, and subsequently calculating the required mean values, one can determine the associated physical quantities and

constants. This analytical approach, centred on mean values, is a standard practice when dealing with statistical systems characterized by a large number of degrees of freedom and inherent randomness.

Experimental Procedure

The objective of this experimental exercise was to determine the Boltzmann constant for two sets of polystyrene micro spheres based on their Brownian motion. The distinguishing factor between the samples was the diameter of the micro spheres: one set comprised spheres with a $1\mu\text{m}$ diameter, while the other set had spheres with a $2\mu\text{m}$ diameter. These micro spheres, procured from Thermo Scientific, were diluted in water to a concentration where numerous spheres exhibited Brownian motion without interacting.

The water-diluted microspheres were placed inside a glass microscope slide to prepare the samples, ensuring the absence of air. Figure 3 provides a sketch of a sample.

To determine the Boltzmann constant, two tasks were crucial. First, we needed to observe and record the Brownian motion of the micro spheres, and second, we had to quantify these recordings for analysis.

We used an experimental setup comprising a microscope with $\times 40$ magnification (Nikon Eclipse E100), a camera (euromex CMEX), and a computer to observe and record the Brownian motion. The camera was positioned over the microscope's output lens to record the sample, and it was connected to a computer displaying a live feed video where recordings were saved. Using this arrangement, we recorded multiple short clips of the Brownian motion of spheres from both samples at a rate of $\approx 30\text{fps}$. There were small fluctuations of $\pm 1\text{ fps}$ in the frame rate which we neglected in our analysis.

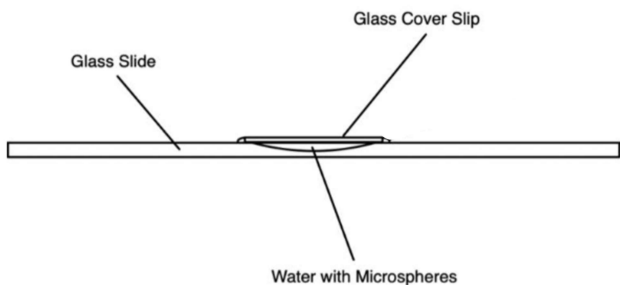


Figure 3: Sample sketch of sample.



Figure 4: Nikon Eclipse E100.

To quantify the recordings, precise information about the spheres' positions at every frame and the relative distances between these positions was necessary. To achieve this, we employed a computer vision software named YoloV8, which could track the micro spheres' positions on the screen for each video frame after we classified selected frames from our videos and ran the annotated screenshots through our Python program utilizing the YOLO library and we run the code for 20000 epoch for the $1\mu\text{m}$ model to establish a well trained but not over trained machine learning algorithm for detecting such particles and for the $2\mu\text{m}$ model we trained the model for 5000 epoch due to time limitations. To ensure accurate distance measurements, the program required calibration with a known distance. For this purpose, we utilized a measuring microscope slide, depicted in Figure 05, to establish the necessary calibration reference.

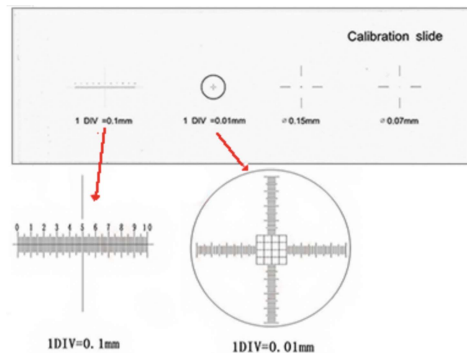


Figure 5: Calibration of the system, utilizing the Micro-Tec MS33 glass calibration slide, 1 mm cross in 0.01mm divisions + 10mm line in 0.1mm divisions + $\varnothing 0.15$ and $\varnothing 0.07\text{mm}$ dots

Utilizing YoloV8, we tracked an adequate number of spheres of each diameter over 30 seconds, acquiring the position points for each sphere that fit our criteria. An illustration of tracking is presented in Figure 06. With the collected data, we can proceed to calculate the Boltzmann constant for each sample.



Figure 6: Tracking of a two $1\mu\text{m}$ micro-spheres that are classified as "dark" with 81% and 98% accuracy respectively with their corresponding particle ids.

YoloV8

Short for "You Only Look Once," YOLO is a model designed for object detection, image classification, and segmentation tasks. It's the latest iteration in the YOLO family, known for its ability to identify objects in an image with just a single analysis pass. YOLOv8 boasts state-of-the-art performance in both speed and accuracy, making it suitable for various applications and adaptable to different hardware, from powerful computers to mobile devices.

For us to be able to start our analysis we need to classify the criteria for a observed particle to be eligible for tracking. After observing the collected videos from the lab we came up with three particle categories.

- "holy"
- "dark"
- "double"

Particles classified as "**holy**" have a distinct feature they appear to have a hole in them. The reasoning for this is simple they are out of the observable range for the specific setting of the microscope at the time of the recording. Thus we have a limited view of their interaction with neighbouring particles that are completely out of the viewing area we are trying to track so by default they are discarded from the tracking and analysis for this experiment. This specific idea for discarding was only applied for the $1\mu\text{m}$ since the $2\mu\text{m}$ videos appear to have only "holy" particles and this is expected to make our results worse.

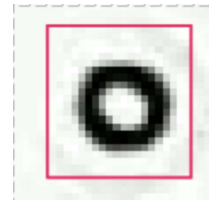


Figure 7: Classification of a "holy" particle.

Particles classified as "**dark**" have distinct features as they aren't distorted by the lens thus their position is not at the edge of the lens's capability. Also quite obviously they are very dark and their borders are well defined. If the criteria above are met then the particle is tracked and will be used for further analysis.

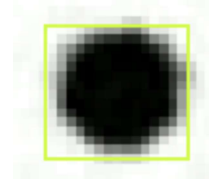


Figure 8: Classification of a "dark" particle.

Particles classified as "**double**" have distinct features. A double pair must be a particle pair or larger in number that is either composed of "**holy**" or "**dark**" particles or a combination of both. These particles are tracked and if they come too close to each other are classified as "**double**". In the case where a "**double**" pair is detected then if the particles were being tracked before that, we stop the tracking and keep the tracked frames of the particles in which they had a few diameters of them self's as a distance from their centres. So "**double**" classification is dependent on the particle sizes. The analysis also excludes all particles classified as "**double**" since they are close enough to each other that their collision is imminent thus their movement stops being random. We were very strict with this criteria since it will greatly affect the data quality and in my opinion, it is crucial even if it greatly reduces the sum of the tracked particles.

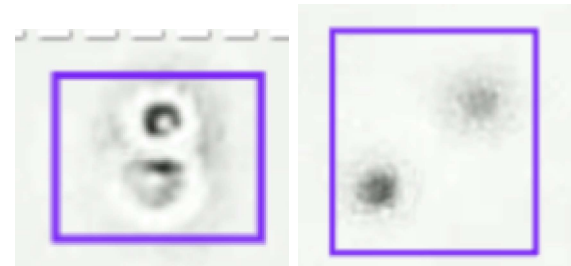


Figure 9: Classification of a "double" particle pair.

A confidence threshold of 0.8 was implemented, thus any classifications with a confidence score lower than 80% were excluded from tracking.

Analysis

From multiple recordings of the Brownian motion exhibited by the polystyrene microspheres in both samples, we tracked many particles of each diameter for 30 seconds. In the tracking process, the position of each sphere was recorded in every frame. Figure 6 and 10 provides an example of one such resulting trajectory.

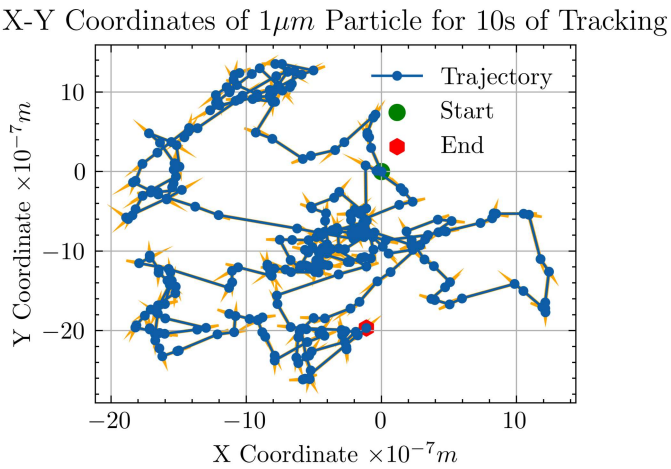


Figure 10: Tracking of a single $1\mu\text{m}$ microsphere in water for 10 seconds.

Before calculating the Boltzmann constant from our dataset, it is crucial to ensure that we have captured pure Brownian motion without any drift velocity resulting from collective liquid movement. The presence of such movement could significantly impact our results, necessitating the rejection of data and a repetition of the data collection process. Pure Brownian motion should exhibit isotropy and complete randomness. To verify the expected nature

of the recorded sphere motion, we can calculate the mean distance from the origin at each time step. Theoretically, this distance should be zero if the motion is genuinely isotropic and random. Any non-zero value would indicate the influence of drift velocity on our data. The results are illustrated in Figures 11 and 12. As the motion in each direction is equivalent, we will analyze the x and y directions separately, obviating the need for vector use during analysis.

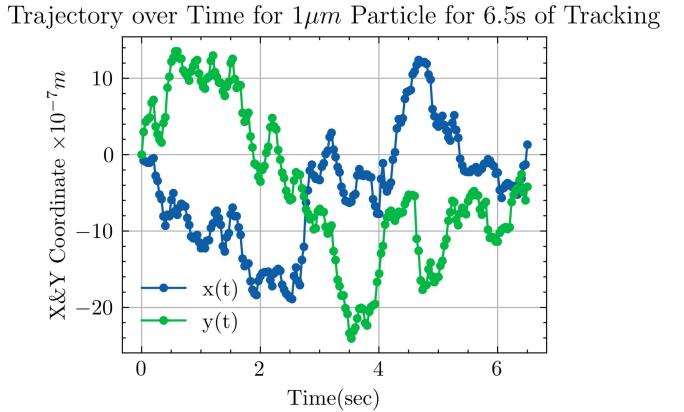


Figure 11: Time evolution of $\langle x \rangle$ and $\langle y \rangle$ for $1\mu\text{m}$ sphere.

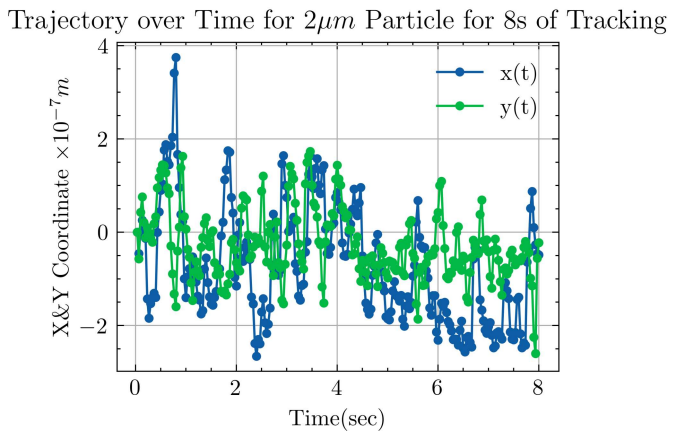


Figure 12: Time evolution of $\langle x \rangle$ and $\langle y \rangle$ for $2\mu\text{m}$ sphere.

Just looking at Figures 11 and 12, it becomes evident that the deviations from the origin are exceptionally small compared to the diameters of the utilized spheres, which measure $1\mu\text{m}$ and $2\mu\text{m}$, respectively. This observation suggests that the recorded motion aligns with expectations of randomness, and the observed deviations are likely statistical. For a more precise quantitative comparison, we intend to assess the mean deviations from the origin after a 10 second motion period, along with their associated uncertainties, against the expected value of zero.

To achieve this, we plan to fit the displacements from the origin after 10 seconds to a Gaussian distribution through a Maximum Likelihood Estimation (MLE) fit. This process will enable us to calculate the uncertainty of the mean value. The uncertainty represents the range of the mean value derived from N spheres undergoing Brownian motion for 1 to 10 seconds. The outcomes of this fitting procedure are presented in Table 1 for 1 second and for the rest in Appendix I, the corresponding fitted distributions can be visualized in Figures 13-16 for the spheres tracked for 1 second.

		Value (μm)	Standard Deviation
Sample 1 (1 sec)	$\langle x \rangle$	-0.060693	0.008598
	σ_x	0.503130	0.008598
	$\langle y \rangle$	0.259442	0.010357
	σ_y	0.635809	0.010357
Sample 2 (1sec)	$\langle x \rangle$	-0.353937	0.059846
	σ_x	1.811392	0.059846
	$\langle y \rangle$	-0.214056	0.063665
	σ_y	1.837906	0.063665

Table 1: MLE Fitting Results.

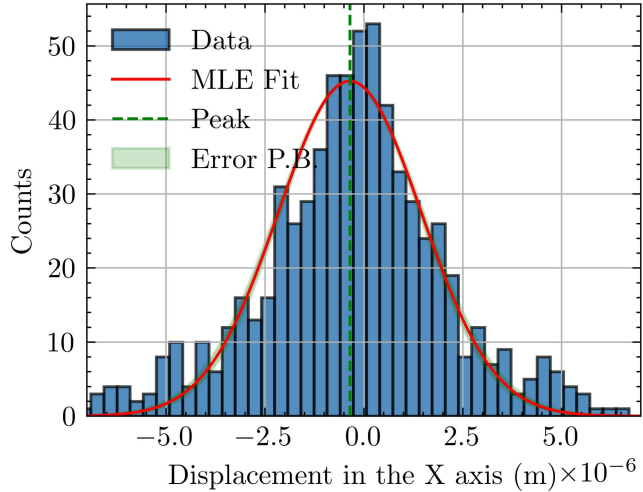


Figure 15: $2\mu m$ spheres x-axis displacements with MLE fitting (Total Spheres: 692).

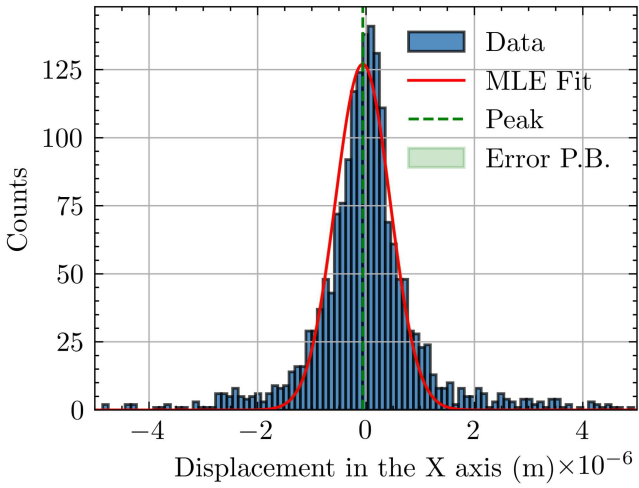


Figure 13: $1\mu m$ spheres x-axis displacements for 1 second with MLE fitting (Total Spheres: 1812).

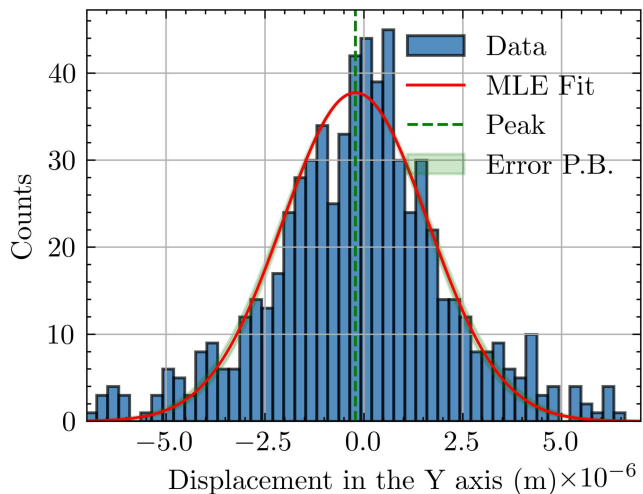


Figure 16: $2\mu m$ spheres y-axis displacements with MLE fitting (Total Spheres: 692).

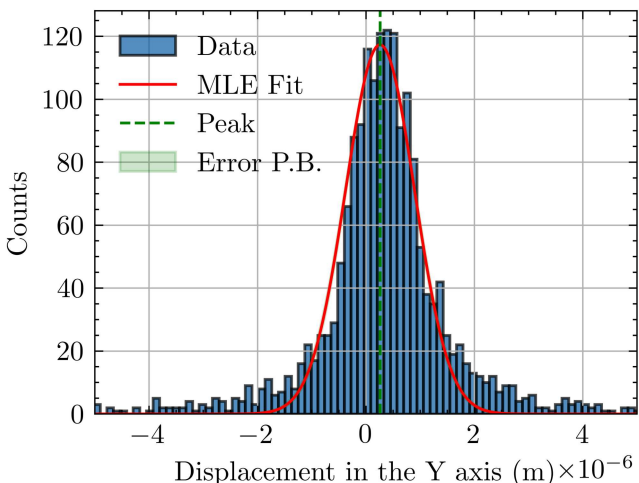


Figure 14: $1\mu m$ spheres y-axis displacements for 1 second with MLE fitting (Total Spheres: 1812).

We are now assured of performing a quantitative assessment, leveraging the mean values derived from 1-10 seconds of motion and their respective uncertainties. It's worth noting that the mean values used in this comparison were obtained through the standard formula, distinct from the fitting procedure.

From our data, we have come to a certain conclusion that in all of the video recordings regardless of the size we have a distinct and slight drift to the y-axis this has led us to believe that because all of the videos have almost identical time evolution for the vectors of drifted speed we suggest that a slight tilt is present in the platform in which we have placed the sample this would perfectly explain the distinct and time dependant drift of the MLE fit peak from the origin in only the y-axis.

Moving forward we calculate the Boltzmann constant for each sample using the following equation:

$$\langle r^2 \rangle = \frac{2k_b T}{3\pi n \alpha} \times t \quad (1)$$

- $\langle r^2 \rangle$ is the mean distance from the origin squared.
- k_b is the Boltzmann constant.
- T is the temperature.
- n is the viscosity of the liquid.
- α is the radius of the sphere.

Equation (1) establishes a connection between the squared mean distance from the origin of a sphere undergoing Brownian motion in two dimensions and measurable physical quantities and constants. The conventional method for addressing random systems involves linking measurable mean quantities with physical parameters. This equation is derived from statistical mechanics and the kinetic theory of gases, with its detailed derivation available in, the work of Jia D. (2007) [6].

We anticipate the variance of the distribution representing the distance from the origin for the microspheres to be as follows:

$$\sigma^2 = \langle r^2 \rangle - \langle r \rangle^2 = \langle r^2 \rangle \quad (2)$$

$$\sigma^2 = \sigma_x^2 + \sigma_y^2 = \frac{2k_b T}{3\pi n \alpha} \times t \quad (3)$$

Given our knowledge and demonstrated proof for Brownian motion, we affirm that the average distance from the origin, denoted as $\langle r \rangle$, is equal to zero.

To determine the Boltzmann constant for each sample, we will employ the following methodology. Initially, we will segment the recorded motion of each particle into four distinct motions characterized by smaller time intervals: 1s, 2s, 3s, 4s, 5s, 6s, 7s, 8s, 9s and 10s. This segmentation is possible as any point in the trajectory can be treated as the starting point for the random motion. Subsequently, we will employ the Maximum Likelihood Estimation (MLE) fit procedure, similar to what was done for previous figures, by fitting Gaussian distributions to the x and y axis displacements from the origin after each time step. Utilizing the resultant variances, we will then perform a least-squares fit to equation (3) to establish its slope. The Boltzmann constant can be computed from this slope, considering that all other physical quantities in the equation are known.

The MLE fit procedure is executed to derive the variances. It is noteworthy that we abstain

from presenting the distributions for each, as they do not offer pertinent information, and comparable examples are evident in past figures but for reference, they are present in Appendix I.

By utilizing the variances from Table 1, we conduct a least-squares fit on equation (3). The outcomes of this fitting process are succinctly summarized in Table 3 and visually depicted in Figures 17 and 18.

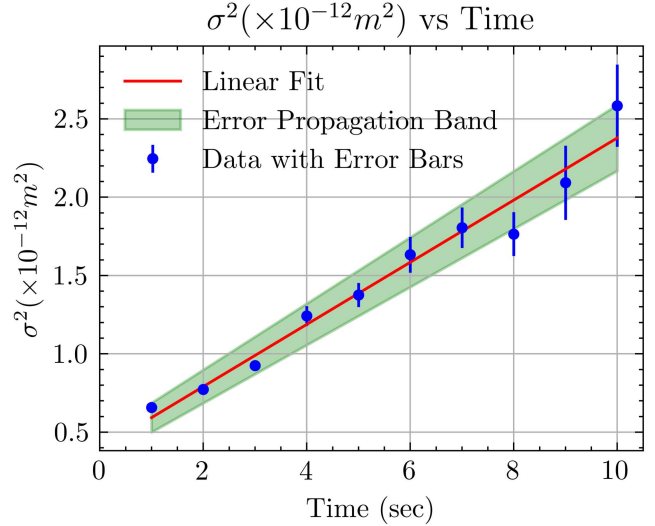


Figure 17: Sample 1 (1μm) Least-Squares Fit.

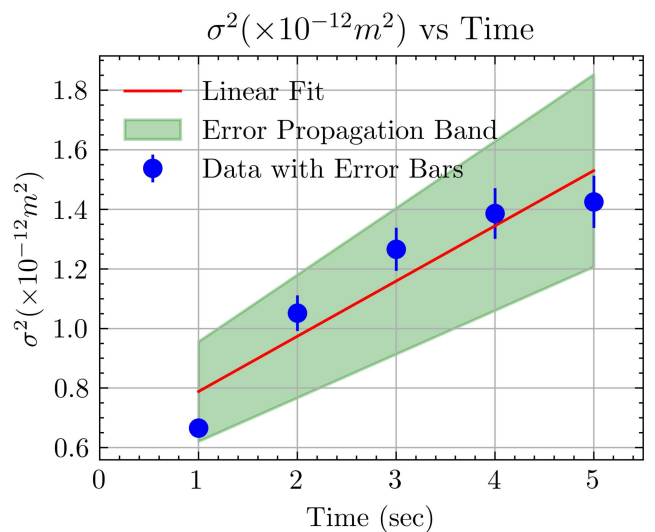


Figure 18: Sample 2 (2μm) Least-Squares Fit.

When solving for the Boltzmann constant from the equation of the slope, we derive the following expression:

$$k_b = \frac{3\pi n \alpha s}{2T} \quad (4)$$

	Time (sec)	Value (μm)
Sample 1	T(K)	300 ± 2
	n(smPa)	0.89 ± 0.005
	$\alpha(\mu\text{m})$	0.5 ± 0.006
Sample 2	T(K)	300 ± 2
	n(smPa)	0.89 ± 0.005
	$\alpha(\mu\text{m})$	1.0 ± 0.012

Table 2: Measured Parameters.

Using the values provided in Table 3 and employing error propagation, we compute the Boltzmann constant for each sample along with their respective standard deviations.

	k_b ($\frac{\text{m}^2 \text{Kg}}{\text{s}^2 \text{K}}$)	Standard Deviation
Sample 1	1.386614×10^{-23}	0.0901×10^{-23}
Sample 2	1.360448×10^{-23}	0.2789×10^{-23}

Table 3: Boltzmann constant Results.

In Table 4, we compare the values obtained through our analysis with the best-known experimental value $k_b = 1.381 \times 10^{-23} \frac{\text{m}^2 \text{Kg}}{\text{s}^2 \text{K}}$

	Percentage Error
Sample 1	0.4323%
Sample 2	1.4701 %

Table 4: Boltzmann constant results comparison.

Based on the findings outlined in Table 3, we can infer that the values we derived for the Boltzmann constant align with the anticipated value, considering the uncertainties inherent in our calculations. The primary factor contributing to uncertainty in our calculations was the variability in the slope we computed, followed by the uncertainty associated with temperature measurements. To enhance the precision of our results, it is imperative to measure the solution temperature and the microscope sample table slope accurately. This will allow us to improve the accuracy of the final result.

Conclusion

In summarizing the experiment's analysis, we observed and monitored the Brownian motion of two microsphere samples with diameters of $1\mu\text{m}$ and $2\mu\text{m}$. The initial data analysis ensured that the recorded motion was genuinely random Brownian motion, unaffected by any large amounts of drift,

as evidenced in Figures 11 and 12. Subsequently, we analyzed and calculated the Boltzmann constant for each sample, presenting the results in Table 3 and comparing them to the best-known experimental value in Table 4. While the Boltzmann constant values were accurate within our measurement uncertainties, the percentage error of around 0.5% & 1.5% suggested that the observed drift didn't affect the precision in our measuring process it just displaced the MLE fitting but didn't interfere with the result. As a means of verifying our model of discarding the "holy" particles, we re-run a few of the videos but with the target of tracking only "holy" particles. This further reinforced our decision to implement such strict criteria due to the results of their tracked trajectories some of them were indeed purely random but a statistically significant number of particles was not resulting in histograms with substantially larger σ_x and σ_y . To enhance precision, further investigation into the cause of the drift speed which is apparent in all the samples regardless of time tracked and video. However, due to the extensive time commitment—approximately 50 hours for training and annotating maybe our machine learning algorithm was lacking and could have been able to track the particles for an even longer period with an even higher confidence rate than 80% which is sufficient but it may have not been best since it may pollute our data with false tracking, but such event wasn't observed. In conclusion, more training would have been helpful since we were able to extract data from both diameters for 10 seconds reliably but the under-trained $2\mu\text{m}$ model produced useless results after 5 seconds of tracking.

References

1. Figure 1 image of Brownian motion from atomic collisions.
2. Figure 4 image of Nikon Eclipse E100.
3. Figure 5 image of Micro-Tec MS33 glass calibration slide & information.
4. YoloV8 website.
5. Water Viscosity Values.
6. Jia D., 2007, 'The time, size, viscosity, and temperature dependence of the Brownian motion of polystyrene microspheres', American Journal of Physics, 75, pp. 111-115

Appendix I

		Value (μm)	Standard Deviation
Sample 1 (1 sec)	$\langle x \rangle$	-0.060693	0.008598
	σ_x	0.503130	0.008598
	$\langle y \rangle$	0.259442	0.010357
	σ_y	0.635809	0.010357
Sample 1 (2 sec)	$\langle y \rangle$	0.388411	0.011707
	σ_y	0.687667	0.011707
	$\langle x \rangle$	-0.064490	0.010440
	σ_x	0.547280	0.010440
Sample 1 (3 sec)	$\langle y \rangle$	0.497913	0.017054
	σ_y	0.767308	0.017054
	$\langle x \rangle$	-0.060661	0.012903
	σ_x	0.580346	0.012903
Sample 1 (4 sec)	$\langle y \rangle$	0.583081	0.028192
	σ_y	0.888766	0.028192
	$\langle x \rangle$	-0.116191	0.020917
	σ_x	0.672302	0.020917
Sample 1 (5 sec)	$\langle y \rangle$	0.571533	0.032641
	σ_y	0.893932	0.032641
	$\langle x \rangle$	-0.070235	0.025891
	σ_x	0.759587	0.025891
Sample 1 (6 sec)	$\langle y \rangle$	0.733049	0.044864
	σ_y	0.999166	0.044864
	$\langle x \rangle$	-0.035768	0.031209
	σ_x	0.796655	0.031209
Sample 1 (7 sec)	$\langle y \rangle$	0.845408	0.048306
	σ_y	1.025778	0.048306
	$\langle x \rangle$	-0.035768	0.055257
	σ_x	0.868040	0.055257
Sample 1 (8 sec)	$\langle y \rangle$	0.871157	0.052652
	σ_y	0.949115	0.052652
	$\langle x \rangle$	-0.085554	0.069225
	σ_x	0.929550	0.069225
Sample 1 (9 sec)	$\langle y \rangle$	0.881181	0.081813
	σ_y	1.043321	0.081813
	$\langle x \rangle$	0.021677	0.071539
	σ_x	1.002161	0.071539
Sample 1 (10 sec)	$\langle y \rangle$	0.853692	0.086413
	σ_y	1.190555	0.086413
	$\langle x \rangle$	-0.056831	0.075654
	σ_x	1.080240	0.075654

Table 1: MLE Fitting Results.

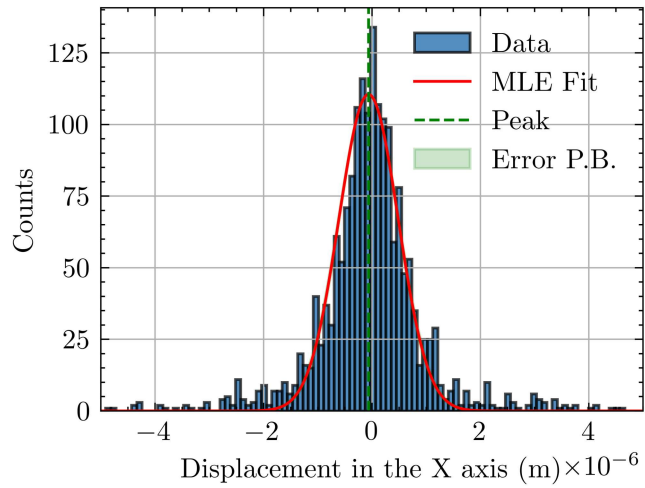


Figure 1: $1\mu m$ spheres x-axis displacements for 2 second with MLE fitting (Total Spheres: 1807).

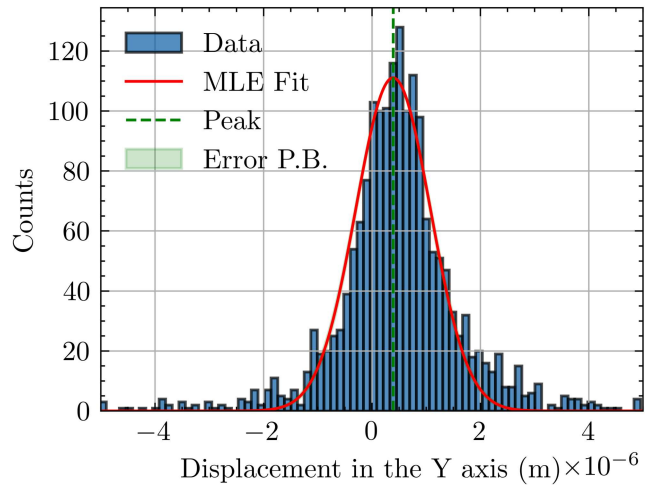


Figure 2: $1\mu m$ spheres y-axis displacements for 2 second with MLE fitting (Total Spheres: 1807)

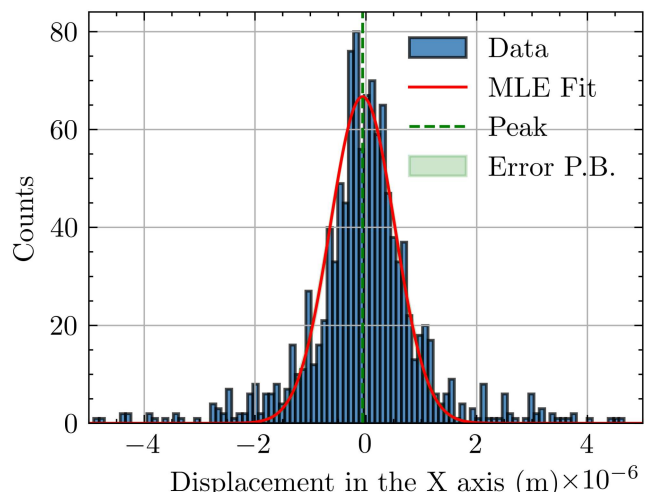


Figure 3: $1\mu m$ spheres x-axis displacements for 3 second with MLE fitting (Total Spheres: 1181).

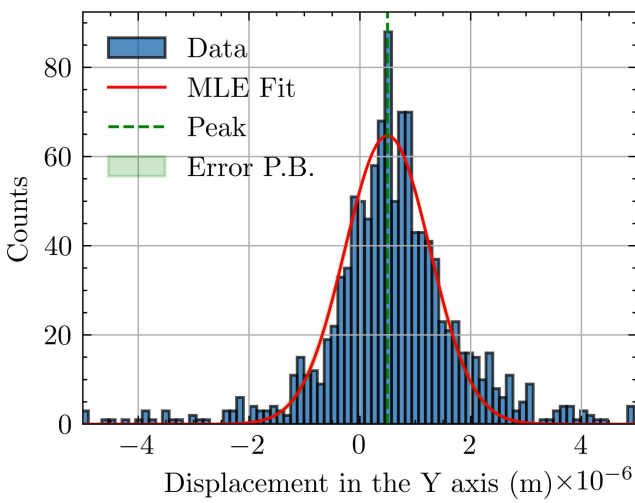


Figure 4: 1μm spheres y-axis displacements for 3 second with MLE fitting (Total Spheres: 1181).

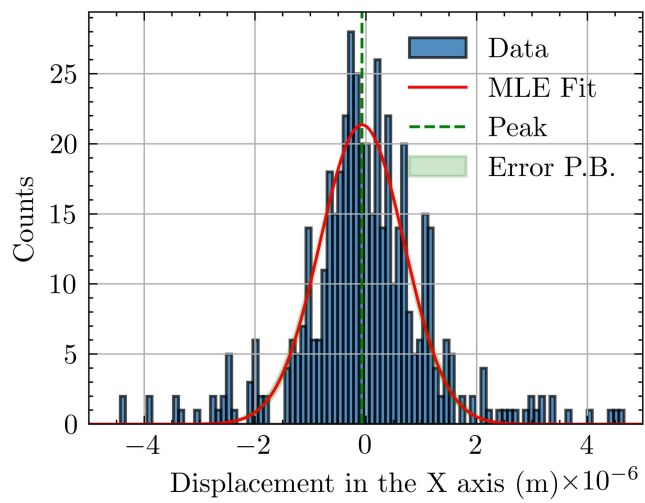


Figure 7: 1μm spheres x-axis displacements for 5 second with MLE fitting (Total Spheres: 479).

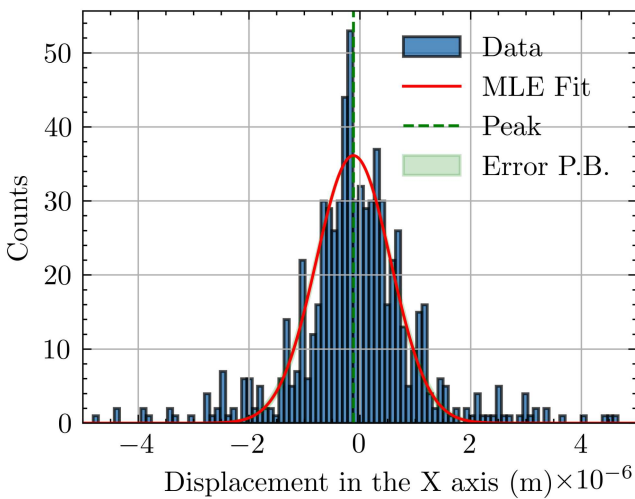


Figure 5: 1μm spheres x-axis displacements for 4 second with MLE fitting (Total Spheres: 728).

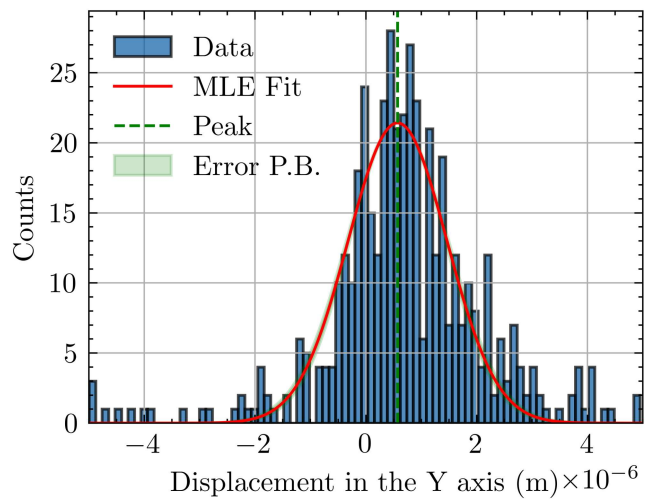


Figure 8: 1μm spheres y-axis displacements for 5 second with MLE fitting (Total Spheres: 479).

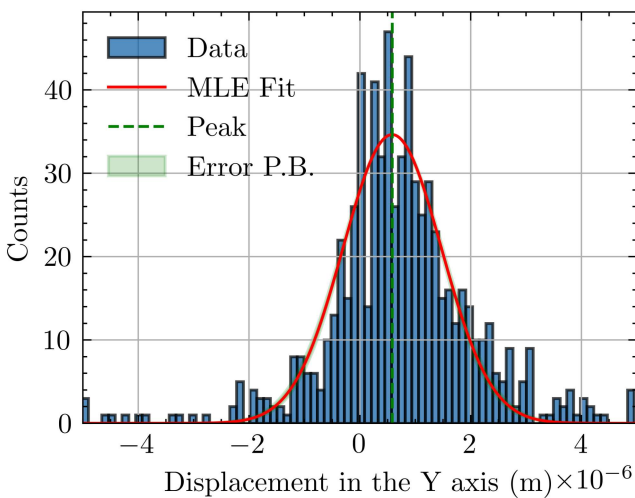


Figure 6: 1μm spheres y-axis displacements for 4 second with MLE fitting (Total Spheres: 728).

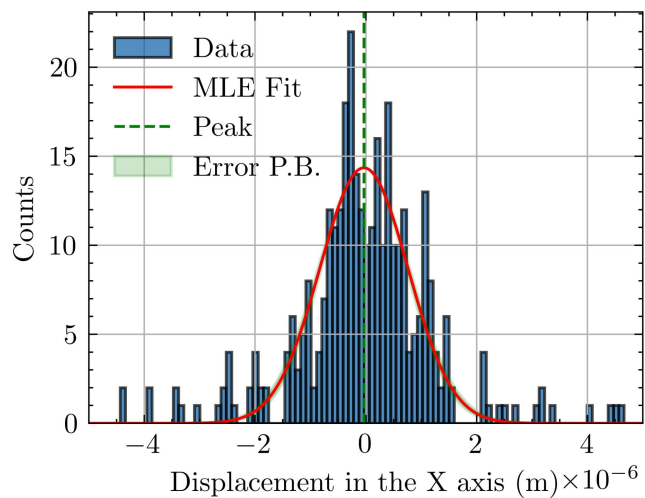


Figure 9: 1μm spheres x-axis displacements for 6 second with MLE fitting (Total Spheres: 339).

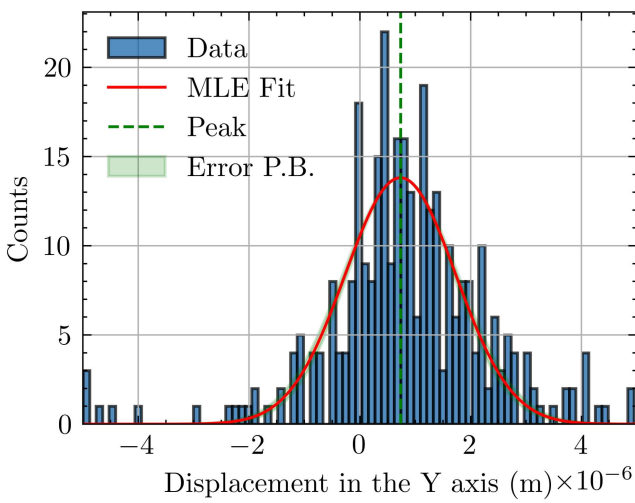


Figure 10: 1μm spheres y-axis displacements for 6 second with MLE fitting (Total Spheres: 339).

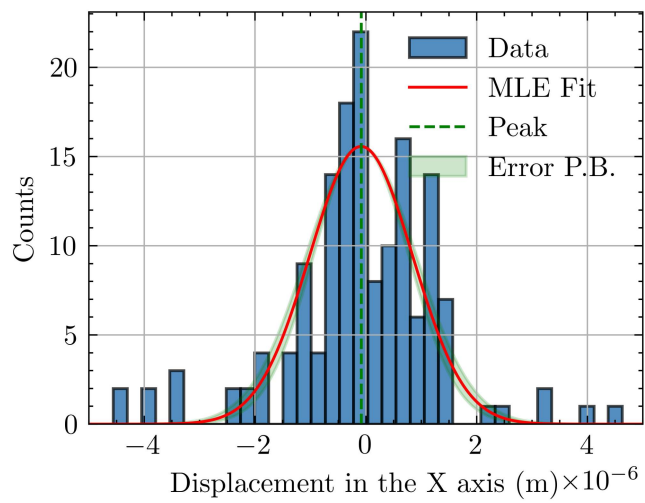


Figure 13: 1μm spheres x-axis displacements for 8 second with MLE fitting (Total Spheres: 161).

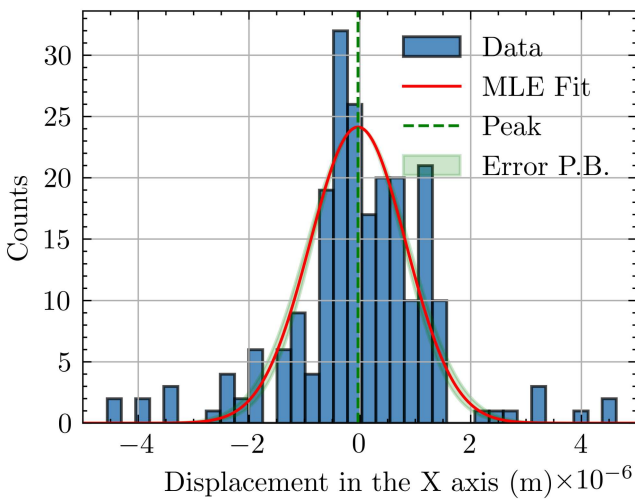


Figure 11: 1μm spheres x-axis displacements for 7 second with MLE fitting (Total Spheres: 232).

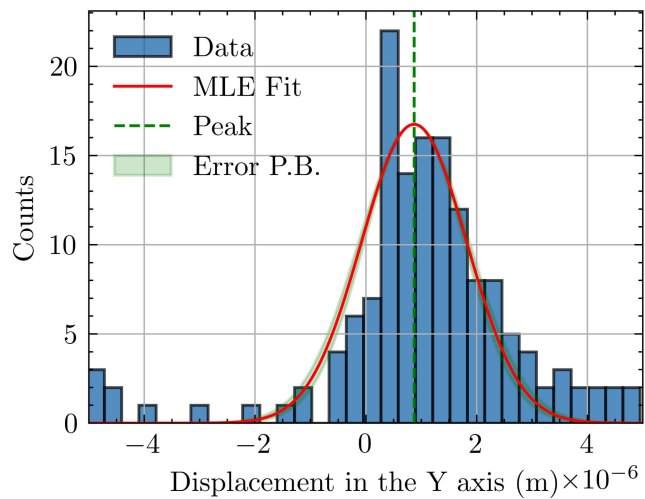


Figure 14: 1μm spheres y-axis displacements for 8 second with MLE fitting (Total Spheres: 161).

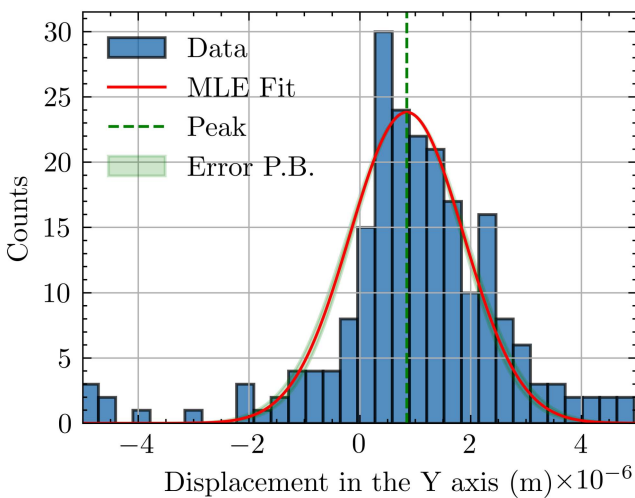


Figure 12: 1μm spheres y-axis displacements for 7 second with MLE fitting (Total Spheres: 232).

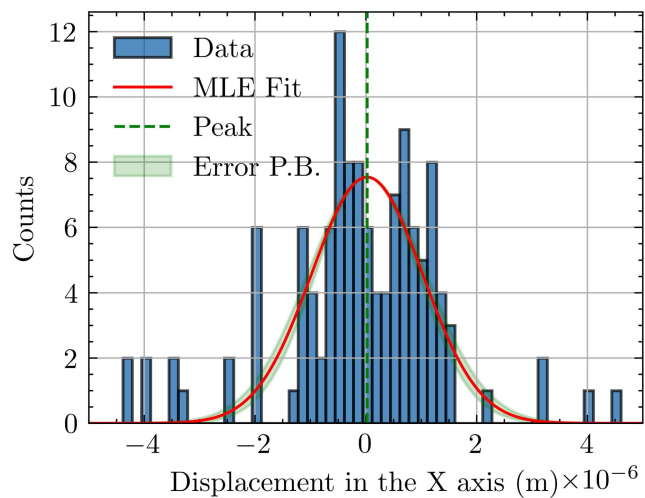


Figure 15: 1μm spheres x-axis displacements for 9 second with MLE fitting (Total Spheres: 129).

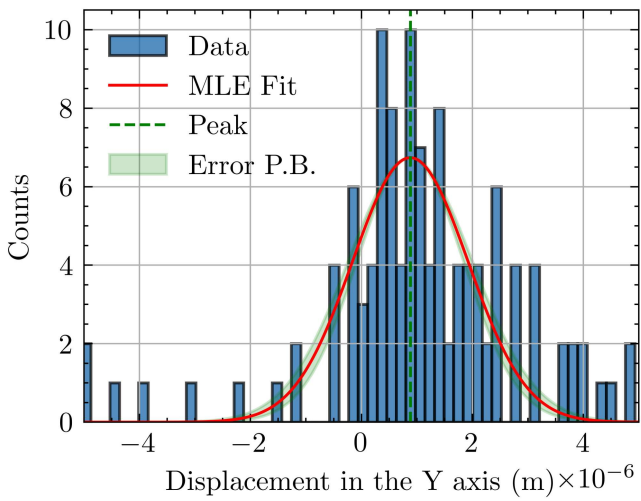


Figure 16: 1 μm spheres y-axis displacements for 9 second with MLE fitting (Total Spheres: 129).

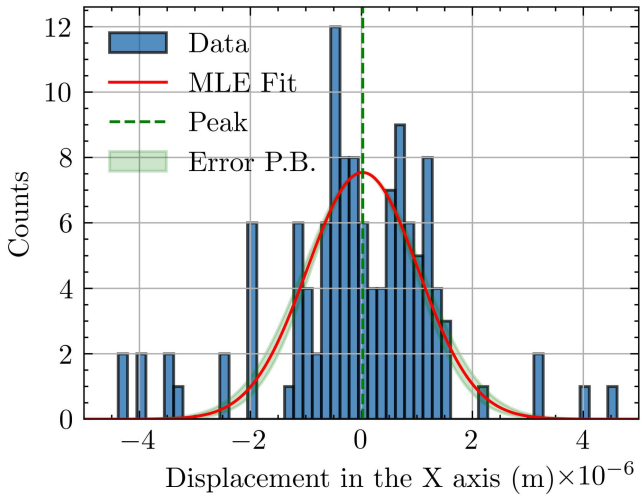


Figure 17: 1 μm spheres x-axis displacements for 10 second with MLE fitting (Total Spheres: 94).

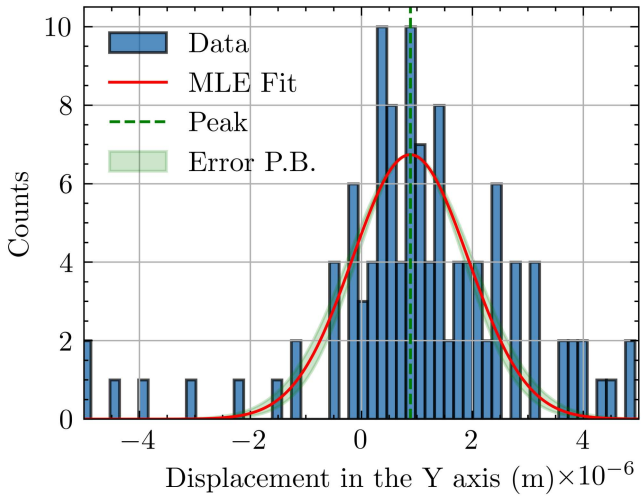


Figure 18: 1 μm spheres y-axis displacements for 10 second with MLE fitting (Total Spheres: 94).

Appendix II

		Value (μm)	Standard Deviation
Sample 2 (1sec)	$\langle x \rangle$	-0.353937	0.059846
	σ_x	1.811392	0.059846
	$\langle y \rangle$	-0.214056	0.063665
	σ_y	1.837906	0.063665
Sample 2 (2 sec)	$\langle y \rangle$	-0.272469	0.090336
	σ_y	2.335956	0.090336
	$\langle x \rangle$	-0.278456	0.094011
	σ_x	2.250005	0.094011
Sample 2 (3 sec)	$\langle y \rangle$	-0.347571	0.100487
	σ_y	2.555779	0.100487
	$\langle x \rangle$	-0.356089	0.103635
	σ_x	2.476218	0.103636
Sample 2 (4 sec)	$\langle y \rangle$	-0.358002	0.113240
	σ_y	2.699782	0.113240
	$\langle x \rangle$	-0.283161	0.114822
	σ_x	2.564491	0.114822
Sample 2 (5 sec)	$\langle y \rangle$	-0.366347	0.119686
	σ_y	2.772138	0.119686
	$\langle x \rangle$	-0.353736	0.111959
	σ_x	2.562899	0.111959
Sample 2 (6 sec)	$\langle y \rangle$	-0.393467	0.205635
	σ_y	2.895855	0.205635
	$\langle x \rangle$	-0.168325	0.202834
	σ_x	2.672056	0.202834
Sample 2 (7 sec)	$\langle y \rangle$	-0.378864	0.146534
	σ_y	2.836039	0.146899
	$\langle x \rangle$	-0.492534	0.147855
	σ_x	2.628833	0.147862
Sample 2 (8 sec)	$\langle y \rangle$	-0.303762	0.161122
	σ_y	2.859960	0.161620
	$\langle x \rangle$	-0.459599	0.139237
	σ_x	2.597737	0.139241
Sample 2 (9 sec)	$\langle y \rangle$	-0.247435	0.162643
	σ_y	2.842112	0.163152
	$\langle x \rangle$	-0.499591	0.144464
	σ_x	2.680069	0.144474
Sample 2 (10 sec)	$\langle y \rangle$	-0.270383	0.163355
	σ_y	2.834482	0.163832
	$\langle x \rangle$	-0.532526	0.148701
	σ_x	2.687964	0.148713

Table 1: MLE Fitting Results.

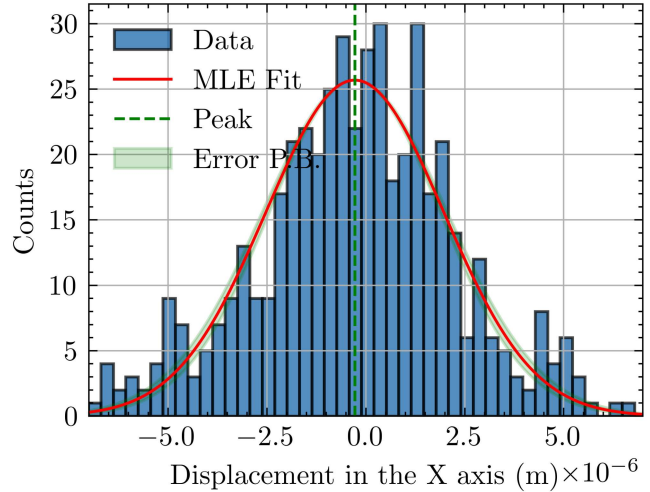


Figure 1: $2\mu\text{m}$ spheres x-axis displacements for 2 seconds with MLE fitting (Total Spheres: 499).

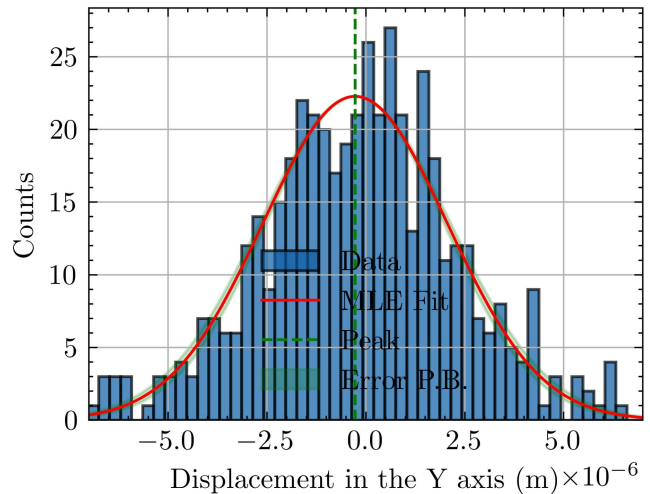


Figure 2: $2\mu\text{m}$ spheres y-axis displacements for 2 seconds with MLE fitting (Total Spheres: 499)

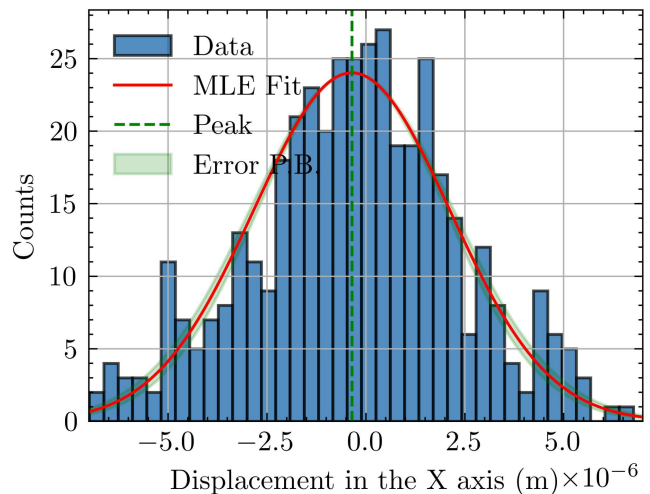


Figure 3: $2\mu\text{m}$ spheres x-axis displacements for 3 seconds with MLE fitting (Total Spheres: 443).

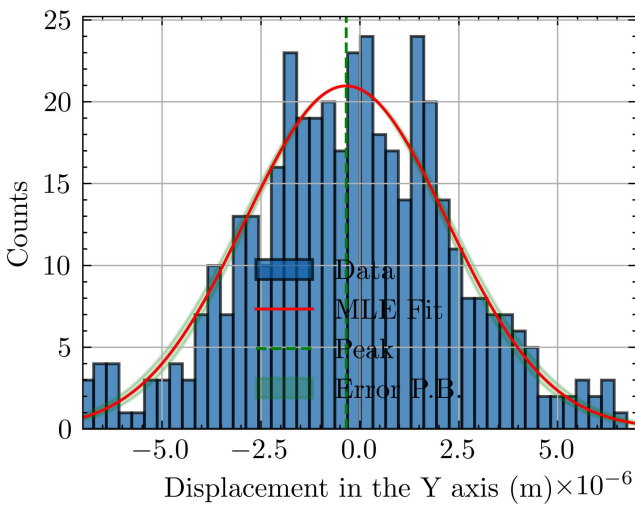


Figure 4: 2 μ m spheres y-axis displacements for 3 seconds with MLE fitting (Total Spheres: 443).

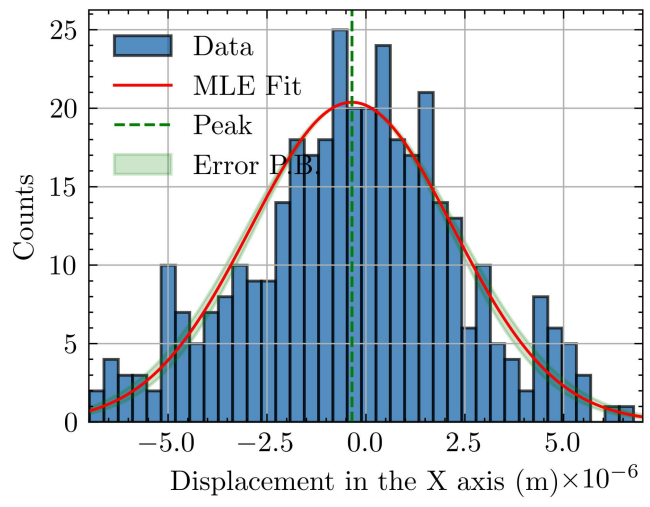


Figure 7: 2 μ m spheres x-axis displacements for 5 seconds with MLE fitting (Total Spheres: 390).

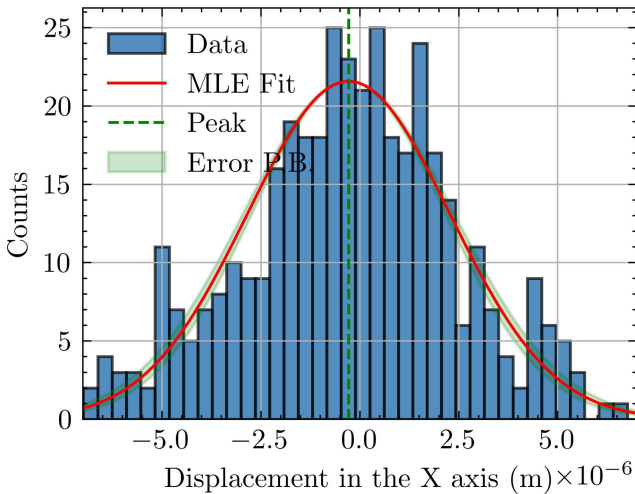


Figure 5: 2 μ m spheres x-axis displacements for 4 seconds with MLE fitting (Total Spheres: 410).

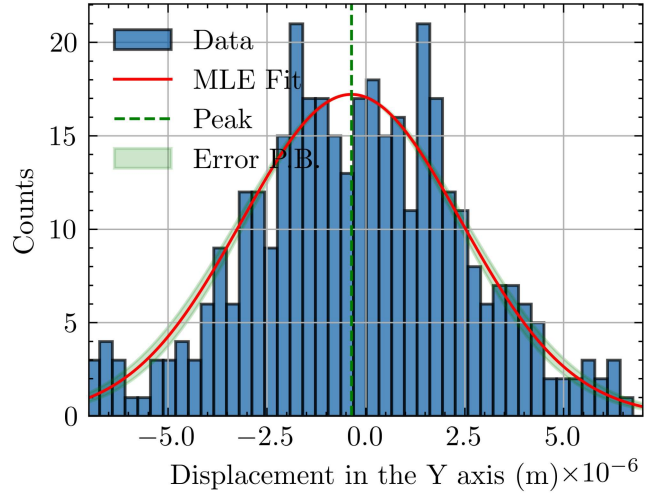


Figure 8: 2 μ m spheres y-axis displacements for 5 seconds with MLE fitting (Total Spheres: 390).

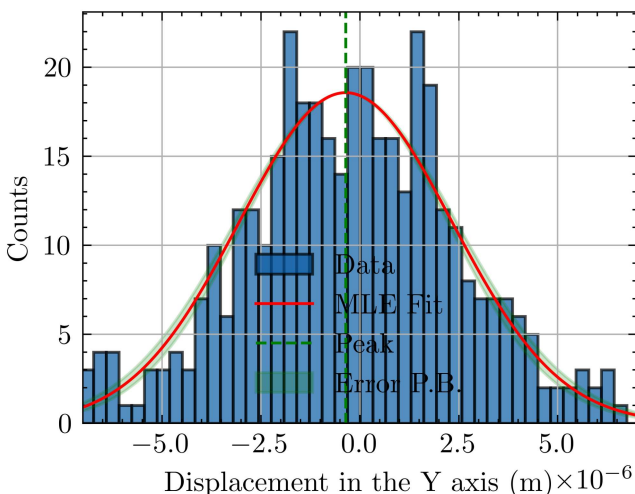


Figure 6: 2 μ m spheres y-axis displacements for 4 seconds with MLE fitting (Total Spheres: 410).

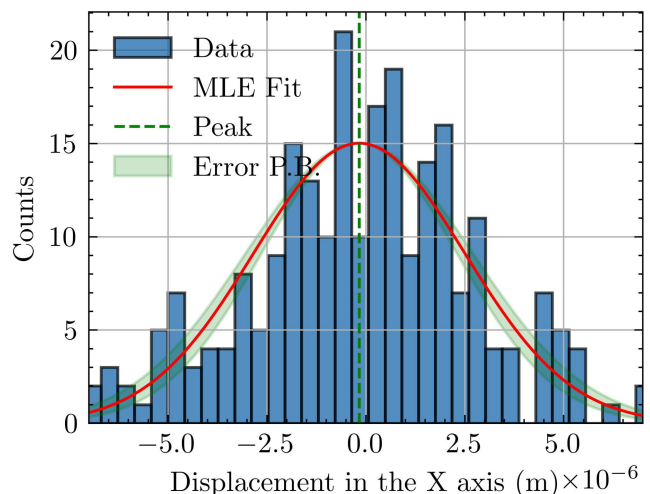


Figure 9: 2 μ m spheres x-axis displacements for 6 seconds with MLE fitting (Total Spheres: 358).

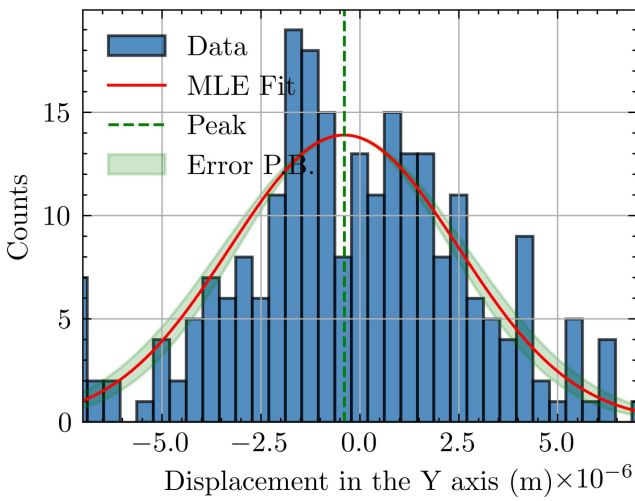


Figure 10: 2 μ m spheres y-axis displacements for 6 seconds with MLE fitting (Total Spheres: 358).

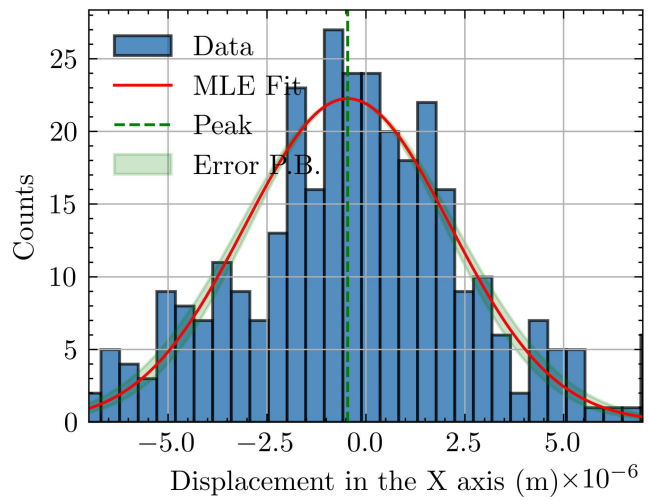


Figure 13: 2 μ m spheres x-axis displacements for 8 seconds with MLE fitting (Total Spheres: 332).

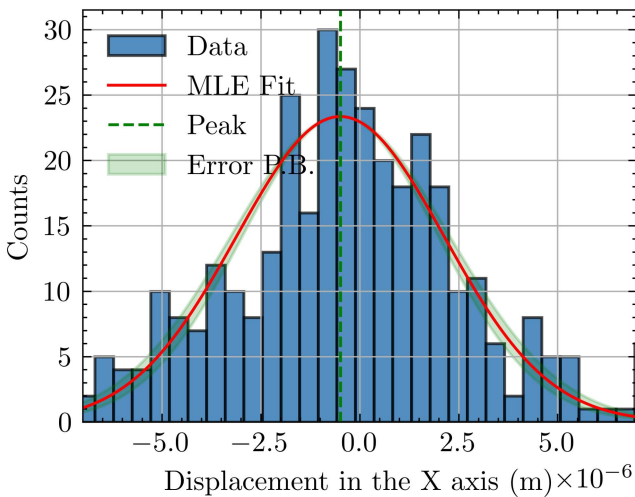


Figure 11: 2 μ m spheres x-axis displacements for 7 seconds with MLE fitting (Total Spheres: 353).

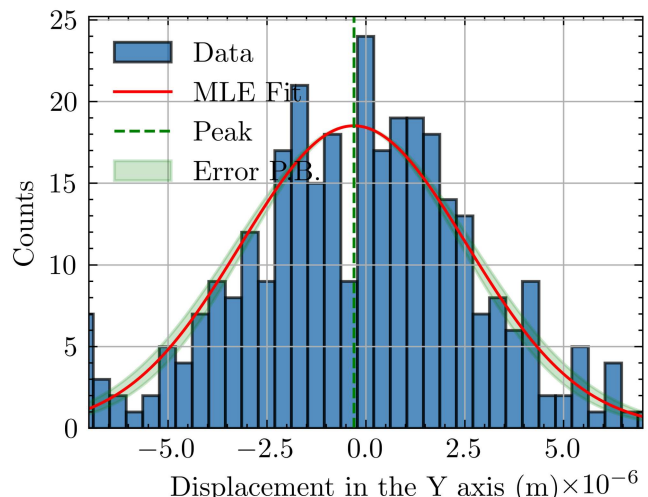


Figure 14: 2 μ m spheres y-axis displacements for 8 seconds with MLE fitting (Total Spheres: 332).

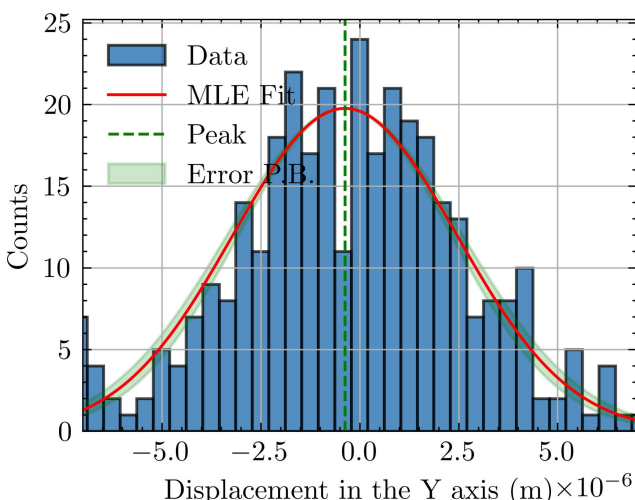


Figure 12: 2 μ m spheres y-axis displacements for 7 seconds with MLE fitting (Total Spheres: 353).

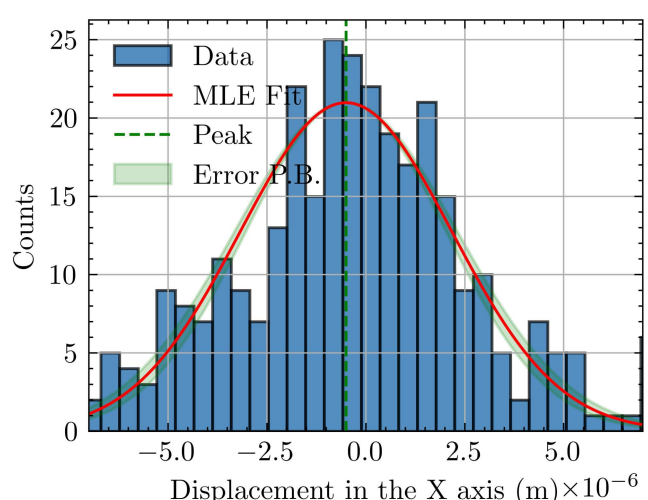


Figure 15: 2 μ m spheres x-axis displacements for 9 seconds with MLE fitting (Total Spheres: 322).

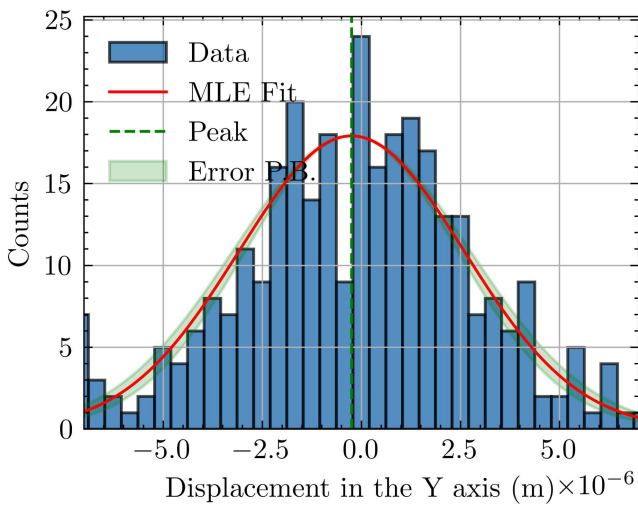


Figure 16: 2 μ m spheres y-axis displacements for 9 seconds with MLE fitting (Total Spheres: 322).

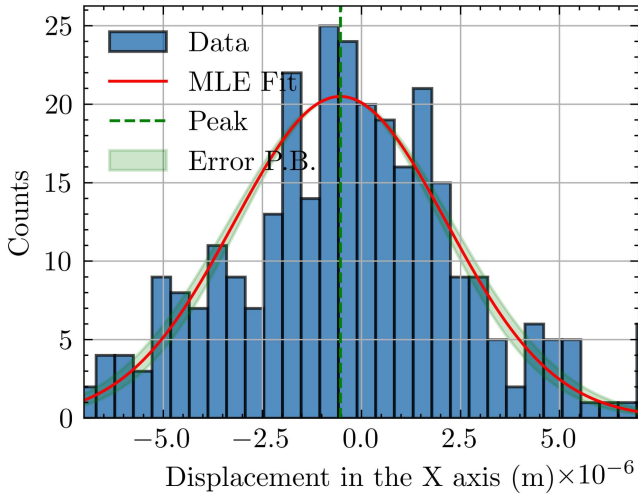


Figure 17: 2 μ m spheres x-axis displacements for 10 seconds with MLE fitting (Total Spheres: 121).

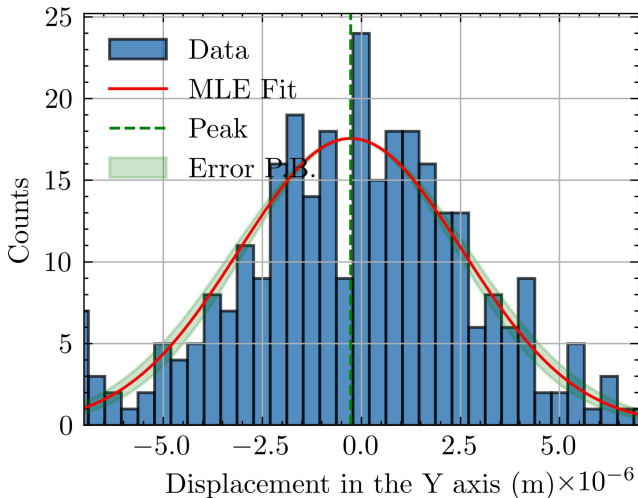


Figure 18: 2 μ m spheres y-axis displacements for 10 seconds with MLE fitting (Total Spheres: 121).